Nanoscale

Photothermal Transformation of Au-Ag Nanocages under Pulsed Laser Irradiation

Journal:	*Nanoscale*
Manuscript ID	NR-ART-12-2018-010002.R1
Article Type:	Paper
Date Submitted by the Author:	21-Jan-2019
Complete List of Authors:	Hood, Zachary; Oak Ridge National Laboratory, Center for Nanophase Materials Sciences (CNMS); Georgia Institute of Technology College of Sciences, Kubelick, Kelsey; Georgia Institute of Technology College of Engineering Gilroy, Kyle; Georgia Institute of Technology, The Wallace H. Coulter Department of Biomedical Engineering Vanderlaan, Don; Georgia Institute of Technology, The Wallace H. Coulter Department of Biomedical Engineering Yang, Xuan; Georgia Institute of Technology, The Wallace H. Coulter Department of Biomedical Engineering Yang, Miaoxin; Georgia Institute of Technology, Chemistry Chi, Miaofang; Oak Ridge National Laboratory, Center for Nanophase Materials Sciences Emelianov, Stanislav; Georgia Institute of Technology , Biomedical Engineering; Georgia Institute of Technology , School of Electrical and Computer Engineering Xia, Younan; Georgia Institute of Technology, The Wallace H. Coulter Department of Biomedical Engineering

Revised MS# NR-ART-12-2018-010002

Photothermal Transformation of Au-Ag Nanocages under Pulsed Laser Irradiation

Zachary D. Hood,[a,b,†] Kelsey P. Kubelick,[c,†] Kyle D. Gilroy,[c,†] Don Vanderlaan,[d] Xuan Yang,[c] Miaoxin Yang,[a] Miaofang Chi,[b] Stanislav Y. Emelianov,[c,d*] and Younan Xia[a,c,*]

[a]School of Chemistry and Biochemistry, Georgia Institute of Technology, Atlanta, Georgia 30332, USA

[b]Center for Nanophase Materials Sciences, Oak Ridge National Laboratory, Oak Ridge, Tennessee 37831, USA

[c]Wallace H. Coulter Department of Biomedical Engineering, Georgia Institute of Technology and Emory University, Atlanta, Georgia 30332, USA

[d]School of Electrical and Computer Engineering, Georgia Institute of Technology, Atlanta, GA 30332, USA

[†]These authors contributed equally to this publication

*Corresponding authors: Stanislav Emelianov (stas@gatech.edu) and Younan Xia (younan.xia@bme.gatech.edu)

Abstract

Pulsed laser irradiation has emerged as an effective means to photothermally transform plasmonic nanostructures after their use in different biomedical applications. However, the ability to predict the products after photothermal transformation requires extensive *ex situ* studies. Here, we report a systematic study of the photothermal transformation of Au-Ag nanocages with a localized surface plasmon resonance at *ca.* 750 nm under pulsed laser irradiation at different fluences and a pulse duration of 5 ns. At biologically relevant laser energies, the pulsed laser transforms Au-Ag nanocages into pseudo-spherical, solid nanoparticles. The solid nanoparticles contained similar numbers of Au and Ag atoms to the parent Au-Ag nanocages. At increased laser fluences (>16 mJ cm^{-2}) and number of pulses (>150), the average diameter of the resulting pseudo-spherical particles increased due to the involvement of Ostwald ripening and/or attachment-based growth. The changes in optical properties as a result of the transformation were validated using simulations based on the discrete dipole approximation method, where the spectral profiles and peak positions of the initial and final states matched well with the experimentally derived data. The results may have implications for the future use of Au-Ag nanocages in biomedicine, catalysis, and sensing.

Keywords: *nanocages · photoacoustic imaging · surface plasmon resonance · plasmonics · contrast agents*

Introduction

Gold-silver (Au-Ag) nanocages with tunable plasmonic properties have received increased research attention owing to their role in biomedical applications, including drug delivery,[1-6] photothermal therapy,[7-10] and imaging.[11-15] Most of prior studies have largely focused on the synthesis and plasmonic properties of Au-Ag nanocages, which is highly dependent on edge length, wall thickness, position and size of the pores, and elemental composition.[16] Thanks to the efforts from many research groups, significant progress has been made to synthesize nanocages with key structural and compositional aspects necessary to enhance biomedical applications.[17-19] Specifically, their optical properties can be easily tuned to absorb light in the near-infrared (NIR) region, facilitating increased light penetration depth for therapy and imaging. In addition to biocompatibility[14, 20] and well-defined bioconjugation protocols,[11, 17, 21, 22] Au-Ag nanocages were recently demonstrated as agents for photothermal therapy and contrast enhancemnt.[3, 13, 23-26] For example, they have been demonstrated for use as a class of exogenous contrast agents toward photoacoustic (PA) imaging. For this imaging modality, optical absorbers are irradiated by pulsed lasers, causing heat deposition and thermoelastic expansion to produce transient pressure waves. The utilization of plasmonic nanoparticles has advanced PA imaging by better facilitating imaging of specific regions or molecular/cellular events of interest.[27-30] To this end, Au-Ag nanocages are of particular interest for their relatively large absorption cross sections (σ_a) in the NIR region and for their ability to efficiently convert light to heat for photothermal therapy due to their tunable localized surface plasmon resonance (LSPR).[31]

Due to their relevance in a variety of applications, plasmonic Au or Ag nanostructures have also been investigated for their photothermal stability and for their structural integrity under pulsed laser irradiation.[32-34] For example, Au nanoparticles,[35, 36] Ag nanodots,[37] Au nanorods,[38] Au nanoshells,[39] and other plasmonic structures[40] have been evaluated for their photothermal stability. Since plasmonic nanoparticles can be quickly heated to relatively high temperatures by lasers with femto-, pico- and nano-second pulse durations, the thermal effects as functions of the pulse energy, laser wavelength, and pulse width are suggested to be primarily responsible for possible photo-fragmentation, melting, and reshaping processes. Various types of Au nanostructures have been evaluated for their stability toward pulsed laser irradiation, but it is still difficult to predict the size and distribution of the resulting particles, necessitating intense experimentation to establish the

structure-stability relationship. The structure-stability relationship is important to the achievement of a better understanding of particle biocompatibility, clearance, and their future role in biomedical applications such as therapeutics, contrast enhancement, and/or diagnostics. Additionally, the structure-stability relationship under pulsed laser irradiation is also beneficial to the development of protocols for synthesizing new metallic nanostructures based on laser ablation.

In the present work, we conducted a set of experiments to explore the photothermal stability of Au-Ag nanocages toward pulsed laser irradiation with fluences below those permitted by the American National Standards Institute (ANSI) at 750 nm.[41] The Au-Ag nanocages with an LSPR peak centered at *ca*. 750 nm were chosen as a model system to match the laser wavelength utilized for the experiments. We monitored the shape or morphological changes by varying different laser parameters, including laser fluence and the number of laser pulses. By varying these parameters, we demonstrate that the changes to the Au-Ag nanocages are both pulse and energy dependent. To better understand the changes, we systematically scrutinized the plausible mechanisms responsible for photothermal transformation using transmission electron microscopy (TEM), energy dispersive X-ray spectroscopy (EDS) analysis, and simulations based on the discrete dipole approximation (DDA) method.

Experimental

Chemicals and Materials

Silver trifluoroacetate (CF_3COOAg, >99.99%), gold(III) chloride trihydrate ($HAuCl_4 \cdot 3H_2O$, ≥99.9%), polyvinylpyrrolidone (PVP, Mw≈55,000), sodium hydrosulfide (NaHS), and hydrochloric acid (HCl, 37 wt.% in H_2O) were all purchased from Sigma-Aldrich. Ethylene glycol (EG) was purchased from J.T. Baker (Batch No. 95444). All chemicals were used as received. Deionized (DI) water with a resistivity of 18.2 MΩ·cm at room temperature was used for all aqueous syntheses.

Synthesis of Ag Nanocubes

The Ag nanocubes with an average edge length of about 45 nm (see Fig. 1A) were prepared using a previously reported protocol.[42] Briefly, 50 mL of EG was preheated at 150 °C for 30 min. During

this time, four separate solutions were prepared: (1) 2.0 mg NaSH in 11.89 mL EG (sample concentration: 3 mM), (2) 3 μL HCl in 12 mL EG (sample concentration: 3 mM), (3) 0.35 g PVP in 17.5 mL EG, and (4) 0.30 g CF_3COOAg (>99.99% metals basis, Aldrich) were dissolved in 4.18 mL EG (sample concentration 282 mM). Each of these solutions was sufficiently stirred to dissolve the reagents. Next, 0.6 mL of (1) was added into EG heated at 150 ^oC. After 4 min, 5 mL of (2) was introduced. After another 2 min, 12.5 mL of (3) was added, and 2 min later, 4 mL of (4) was added. The synthesis was terminated by cooling the solution in an ice bath after 60 min into the reaction. The Ag nanocubes were purified by dispersing the solid products in acetone and then collected by centrifugation at 4,900 rpm for 8 min. The Ag nanocubes were washed three times in DI H_2O, collected by centrifugation at 14,000 rpm for 15 min, and dispersed in 8 mL of DI H_2O to create a stock solution of Ag nanocubes.

Synthesis of Au-Ag Nanocages

The Au-Ag nanocages (see Fig. 1B) were prepared *via* a galvanic replacement reaction between Ag nanocubes and $HAuCl_4$.[43] Briefly, 1 mL of the stock solution of Ag nanocubes was added into 20 mL of DI H_2O and heated at 90 ^oC for 20 min. A freshly prepared stock solution of $HAuCl_4$ (0.75 mM, 20 mL) was loaded in a syringe (BD plastic, 30 mL) and titrated into the suspension of Ag nanocubes at a rate of 4.5 mL h^{-1}. The reaction was monitored by UV-vis spectroscopy, and once the LSPR reached ~750 nm, the reaction was terminated by cooling in an ice water bath, stirred for 1 h with excess NaCl to remove AgCl, and centrifuged at 10,000 rpm for 20 min. The pellet containing Au-Ag nanocages was washed five times by re-dispersing in 25 DI H_2O and centrifuging at 10,500 rpm.

Pulsed Laser Irradiation

Figure 1C shows a photograph of the experimental setup used for pulsed laser irradiation. The samples were irradiated using a Nd:YAG laser pumped with a tunable OPO laser system (Phocus, Opotek Inc.) operated at a wavelength of 750 nm, 5-7 ns pulse duration, and 10 Hz repetition rate with a spectral linewidth of the pulsed laser between 30–80 cm^{-1}. A 96 well plate with a clear bottom and black sides was loaded with 50 μL of an aqueous dispersion of the Au-Ag nanocages at an optical density of 0.5. For each experiment, the laser fluence and number of pulses were controlled using an automated lasing system, developed in-house. Fluence was set between 0–30 mJ cm^{-2}, and the number of laser pulses was set between 5–300 pulses. The optical fiber was

positioned above each individual well such that the laser spot size irradiated the entire solution while the adjacent wells were not irradiated. All pulsed laser experiments were conducted at room temperature.

Characterization

All UV-visible spectra were collected using a spectrophotometer (Synergy HT microplate reader, BioTek Instruments) between 400 and 900 nm, and the metal contents were quantified using inductively-coupled plasma mass spectrometry (ICP-MS, NexION 300Q, Perkin Elmer). Transmission electron microscopy (TEM) images were collected on a Hitachi HT7700 operated at 120 kV after dispersing 4 μL of an aqueous suspension of each sample on carbon-coated copper TEM grids. All TEM images were analyzed using ImageJ in order to generate statistical data for the different nanomaterials. The size distribution was determined by measuring >150 particles. High-angle annular dark-field (HAADF) and bright-field (BF) scanning transmission electron microscopy (STEM) imaging and energy-dispersive X-ray spectroscopy (EDS) were completed on an aberration-corrected JEOL JEM 2200FS STEM/TEM microscope operated at 200 kV, equipped with a CEOS probe detector (Heidelberg, Germany) and a Bruker-AXS silicon drift detector (SDD).

Discrete Dipole Approximation Simulations

To simulate the optical properties of the nanoparticles before and after laser irradiation, we used experimentally measured dimensions to approximate the design of two continuum models: (1) Initial state–a box with an edge-length of 47 nm, wall thickness of 4 nm, and spherical pores etched from each of the corners with a radii of 10 nm; resulting in a structure with an effective radius (r_{eff}) for the entire structure estimated to be around 20.5 nm, see the inset of Figure 2B for an illustration of the nanocage and refer to the SI for how the shape was created; and (2) final state–a sphere with a radius of 21 nm and 33401 dipoles. For both simulations, the dielectric constant was approximated for $Au_{52}Ag_{48}$ by extracting the values from ref. 44 (see Fig. S1 for the reproduced dielectric constant), which provides dielectric constant data for AuAg alloys with various molar ratios.

Results and Discussion

The Au-Ag nanocages were synthesized using galvanic replacement between $HAuCl_4$ and Ag nanocubes at 90 °C, as described in previous reports.[42, 43] In short, Ag nanocubes with an edge length of 45 nm (Figs. 1A and S2) were transformed into nanocages by slowly adding an aqueous solution of $HAuCl_4$ into the suspension. TEM images were captured from the as-prepared Au-Ag nanocages, indicating an average edge length of ~47 nm, together with a wall thickness of ~4.5 nm and well-defined pores of 4–6 nm in size (Figs. 1B, S2-S4). These data correspond to an average volume of about 49000 nm^3 for each nanocage. The ICP-MS data indicate that the as-prepared nanocages were composed of 51.3% Au and 48.7% Ag, similar to previous reports.[43, 45]

Figure 1C shows a photograph of the experimental setup used for pulsed laser irradiation. A 96-well plate was loaded with an aqueous dispersion of the Au-Ag nanocages (50 μL) with an optical density of 0.5. For these experiments, optical density served as a simple parameter to measure the particle concentration in terms of light attenuation at a specific wavelength. At this volume and optical density, light attenuation was calculated to be less than 10% throughout the sample. The optical fiber was aligned to produce a laser spot size of 6 mm in diameter, which roughly corresponds to the diameter of each well. As such, the entire sample was assumed to be equally irradiated. The black plastic between adjacent wells prevented unintentional exposure.[46] The laser fluence was tuned in the range of 0–30 mJ cm^{-2} while the number of laser pulses was varied between 5–300 pulses to allow for a systematic examination of the structure-stability relationship of Au-Ag nanocages upon exposure to pulsed lasers at biologically relevant energies (*i.e.*, at levels permitted by ANSI).

We first analyzed the energy-dependent optical and morphological changes after the nanocages had been exposed to 300 laser pulses with fluences between 4–30 mJ cm^{-2}. After laser irradiation, a sharp peak appeared at 460 nm, whose relative intensity increased with laser fluence (Fig. 2A). Figures 2C-E show the corresponding TEM images of the nanocages before and after 300 laser pulses at 4 and 20 mJ cm^{-2}, respectively. After 300 pulses at a laser fluence of 4 mJ cm^{-2}, most of the nanocages remained, but their overall size was significantly reduced relative to the as-prepared Au-Ag nanocages (the edge length decreased to 37 nm, with a wall thickness of about 7 nm) with barely noticeable pores at the corners (Fig. 2D). Increasing the laser fluence to 20 mJ cm^{-2} caused the nanocages to significantly change their shape, resulting in pseudo-spherical nanoparticles, as

schematically shown in Figure 2F.

We further used EDS with STEM imaging to analyze the compositions of the nanocages and pseudo-spherical nanoparticles. As shown in Figure 3, EDS elemental mappings of Au and Ag in the as-prepared Au-Ag nanocages indicated that the walls were composed of Au-Ag alloys, in agreement with ICP-MS result. After 300 pulses at a laser fluence of 12 mJ cm^{-2}, the resulting nanoparticles were nearly spherical. As highlighted in the EDS elemental mapping, the spherical particles were composed of an alloy made of Au and Ag with compositions similar to those of the starting Au-Ag nanocages (Fig. 3F). Additionally, ICP-MS analysis indicates that the pseudo-spherical, solid nanoparticles contained 51% Au and 49% Ag. Thus, the absorbance peak at 460 nm was due to the plasmon resonance of the pseudo-spherical Au-Ag alloy nanoparticles rather than pure Ag nanoparticles such as those produced using laser ablation.[47-51]

To gain more insight into the evolution of the UV-vis spectra measured from the experiments, simulations based on the DDA method were used to estimate the extinction spectra of the modeled structures (nanocage and pseudo-spherical solid nanoparticle) in water (n = 1.33). For both cases, we used a dielectric constant of $Au_{52}Ag_{48}$ derived from ref. 44 and the reproduced dielectric constant can be found in Figure S1. The $Au_{52}Ag_{48}$ nanocages, with an edge length of 47 nm, wall thickness of 4 nm, and 10 nm spherical pores, had an LSPR extinction peak centered at ~774 nm, which is in reasonable agreement with the broad peak experimentally observed in the region of 750 nm. We then simulated the optical spectrum of 41-nm pseudo-spherical, solid $Au_{52}Ag_{48}$ nanoparticles to represent the nanoscale products after photothermal transformation. We selected a diameter of 41 nm because it is approximately equivalent to the effective diameter of the simulated nanocage in terms of mass. Modeling results showed a peak position at 472 nm, which was similar to the experimental value at 460 nm. In addition to having an agreement in both peak position and overall spectral profile, it was clear that the ratios between the theoretical and experimental peak intensities (nanocage over pseudo-spherical nanoparticle) also agreed reasonably well (2.3 *versus* 1.7, respectively).

After 300 laser pulses at a fluence of 8, 12, and 20 mJ cm^{-2}, the average diameter was measured for the resulting Au-Ag alloy pseudo-spherical nanoparticles and it was found to increase as the laser fluence increased (Fig. S5). Analysis of the volume changes revealed that, on average, the pseudo-spherical nanoparticles with an average diameter around 45 nm had a mass similar to that

of the starting nanocages. When the laser fluence was increased to 8 or 12 mJ cm^{-2}, most of the resulting pseudo-spherical, solid nanoparticles had a diameter in the range of 40–45 nm, but when the laser fluence was increased to 20 mJ cm^{-2}, the average diameter of the pseudo-spherical, solid nanoparticles increased, implying that some of the nanoparticles might have fused together through Ostwald ripening and/or attachment.

Under the conditions used in the current study, the Au-Ag nanocages appeared to change their shape at the same rate at a relatively low laser fluence (*e.g.* 4 laser fluences mJ cm^{-2}) whereas the process appears to be stochastic at laser fluences >8 mJ cm^{-2}. At a laser fluence of 20 mJ cm^{-2}, the samples were more heterogeneous with a broader particle size distribution. This result can be attributed to Ostwald ripening and/or attachment-based growth due to the significantly higher energy present in the system. It should also be noted that more Ostwald ripening and/or attachment-based growth would be expected at increased concentrations of Au-Ag nanocages under the same conditions for pulsed laser irradiation. Thermal coupling due to decreasing inter-particle distance at higher particle concentrations may also impact the transformation of the Au-Ag nanocages into pseudo-spherical, solid particles.

To understand the atomic rearrangement after the transition from nanocage to pseudo-spherical nanoparticle, STEM images were recorded for the particles after 300 pulses at a laser fluence of 12 mJ·cm^{-2} and a representative particle is shown in Figure 4. The STEM images clearly show that the pseudo-spherical nanoparticle was polycrystalline, suggesting the following possibilities: (1) planar defects (*e.g.*, stacking faults) were generated during the rapid heating and cooling process, (2) coalescence occurred during the photothermal reshaping process, or (3) a combination of both processes.[52] The difference in effective volume between the initial and final states was only 5%, suggesting that coalescence was minimal. Furthermore, the bright-field STEM images in Figure 4, C and D, show the presence of planar defects in the resulting pseudo-spherical nanoparticles. The polycrystalline nature of the pseudo-spherical nanoparticle also indicates that the mechanism for generating these particles involves both physical and chemical processes due to the nature of pulsed laser photothermal heating.[53] It is possible that pulsed laser irradiation generates a mixture of atomic clusters, and subsequently produces areas where the vapor pressure of ablated species is greater than their equilibrium vapor pressure close to room temperature, hence nucleation rapidly occurs for the generation of polycrystalline pseudo-spherical nanoparticles. Since surface atoms

are less stable, these atoms are susceptible to surface reconstruction during the electron-photon relaxation.

The number of laser pulses also played an important role in the reconstruction of the Au-Ag nanocages to pseudo-spherical nanoparticles. Since 300 laser pulses at a fluence of 8 mJ cm^{-2} provided sufficient energy to transform the Au-Ag nanocages for the observation of a decrease in the LSPR peak at 750 nm and an increase in the LSPR peak at 460 nm, for the next set of experiments, we held laser fluence constant at 8 mJ cm^{-2} while increasing the number of pulses from 5 and 300. Figure 5 shows TEM images of the resulting nanoparticles after 5, 50, 150, and 300 pulses. Increasing the number of laser pulses led to a greater percentage of pseudo-spherical, solid particles in the resulting sample. Some Au-Ag nanocages and nanoframes were found in the solution after 5, 50, and 150 pulses, demonstrating that a large number of photons was necessary to cause the total surface energy to reduce during pulsed laser photothermal heating. Furthermore, this result suggests that the degree of transformation can be tuned by changing the combinations of pulse number and laser fluence.

It has been reported that reconstruction and/or melting can start from the surface of a metal nanoparticle at a greatly reduced temperature relative to the bulk material,[54, 55] especially when the nanoparticle is heterogeneously heated. The surface atoms are generally less stable in a metallic nanostructure, leading to surface reconstruction at a relatively low temperature. For example, in the study of Au nanorods, it was shown that particle reconstruction occurred as a result of surface pre-melting and the introduction of defects within the nanorod during pulsed laser irradiation.[56] Depending on the pulse duration, wavelength, and pulse energy, Au nanorods were previously shown to melt/transform into spherical nanoparticles with different sizes.[38, 56] More recently, the heat dissipation rate was shown to have a strong correlation to the final morphology of Au nanorods. Using femtosecond pulsed lasers at fluences of 0.32–0.38 mJ/cm^2, González-Rubio *et al.* have shown that lower cooling rates lead to significant changes in the morphology of Au nanorods, whereas fast cooling had minimal effect on the morphology.[57] The surface density of the surfactant on the Au nanorods was also crucial in controlling heat dissipation and the resulting morphology. In contrast to nanorods, nanocages have a relatively higher percentage of surface atoms due to their hollow and porous morphology. Therefore, the surface atoms are primarily expected to participate in the photothermal transformation of the nanocages during pulsed laser

irradiation, especially at higher laser fluences. To this end, future studies of the photothermal stability and transformation of Au-Ag nanocages within the fluence range 0.1–1.0 mJ/cm^2 using nano/femtosecond lasers, as well as different surfactants, may yield interesting results in their morphology and optical properties.

The exact mechanism responsible for the photothermal transformation of Au-Ag nanocages to pseudo-spherical, solid nanoparticles is yet to be fully understood. One possible mechanism involves multiphoton ionization of atoms in Au-Ag nanocages upon irradiation with a nanosecond laser. This process causes electrostatic repulsion between the atoms in the nanocages, leading to transformation from a hollow nanocage to a solid sphere can help minimize the electrostatic repulsion between charges in ionized nanoparticles (Figure S6). A second possible mechanism involves heating the electrons in the Au-Ag nanocages through the initial photon absorption, which occurs on the femtosecond time domain.[38, 58, 59] After initial photon absorption, the atoms in the nanocages undergo electron-phonon relaxation, resulting in lattice heating and vibrations and thus transformation of the nanocages as summarized below:

$$\text{Au-Ag}_{\text{NC}} \xrightarrow{nh\nu} [\text{Au-Ag}_{\text{NC}}]^{\text{vib}} \xrightarrow{melting} \text{Au-Ag}_{\text{NS}}$$

During pulsed laser irradiation, the total surface energy will be reduced during the morphological transformation from nanocages (NC) to near-spherical (NS) nanoparticles with a solid structure. The electron-phonon relaxation occurs on the picosecond time domain and homogeneously heats the Au-Ag nanocages, inducing a morphological change. It must be stressed that the pulse lengths in the current work are nanosecond in duration, thus providing sufficient energy to cause these effects. In previous studies of Au nanorods[38] and Au nanoparticles,[35, 36] nanosecond laser pulses were shown to fragment the nanostructures into smaller particles. This result was explained on the basis that further excitation of the hot lattice with nanosecond laser pulses would lead to the absorption of more photons by the hot lattice, causing the lattice internal energy to increase and thus leading to fragmentation of the nanostructures. As evident from the results under the laser conditions in the present work, photothermal reshaping of Au-Ag nanocages was preferred over fragmentation.

An understanding of the photothermal stability of Au-Ag nanocages has implications for a number of fields. In biomedicine, Au-Ag nanocages have the potential to be used as exogenous

contrast agents in PA imaging, and the utilization of a pulsed laser for PA imaging will likely cause the Au-Ag nanocages to reshape under the conditions used in this study. Therefore, future studies detailing methods to increase the photothermal stability of Au-Ag nanocages and related structures will be important for the development of future exogenous contrast agents for PA imaging. Additionally, the study of Au-Ag nanocages in tissue-like phantoms will be important for understanding the heat dissipation from the nanostructure as well as the effect of the phantom towards Ostwald ripening and/or attachment-based growth of the embedded nanostructures. In materials science and chemistry, laser ablation is widely used to synthesize nanostructures with unique morphologies and properties. Our results demonstrated that pulsed laser irradiation could be used to transform Au-Ag nanocages into polycrystalline nanoparticles with planar-defects, which may find use in heterogeneous catalysis and related applications.

Conclusion

We have systematically investigated photothermal transformation of Au-Ag nanocages under pulsed laser irradiation on the basis of surface plasmon resonance, structure, and chemistry. Specifically, Au-Ag nanocages were found to transform into pseudo-spherical, polycrystalline nanoparticles of comparable volumes after 300 pulses of laser irradiation (5 ns pulse duration, 10 Hz frequency) at a laser fluence of 4–30 mJ cm^{-2}. It was found that the pulse energy and number of pulses both affected the resulting morphology of the Au-Ag nanocages. Under pulsed laser irradiation, the atoms diffused across the surface of the nanocages, and when enough energy was present, pseudo-spherical nanoparticles emerged as the thermodynamic products. The electron-phonon relaxation allowed the nanocages to be heated homogenously, causing them to reshape and evolve into pseudo-spherical, solid nanoparticles when enough energy was supplied. The experimentally-derived optical and structural data agreed well with those derived from theoretical simulations based on the DDA method in terms of spectral profile and peak position. We believe this work will stimulate further investigation into the thermal stability of hollow metal nanostructures and the applications thereof.

Conflicts of interest

The authors have no conflicts to declare.

Acknowledgments

A portion of this research was conducted at the Center for Nanophase Materials Sciences, which is a DOE Office of Science User Facility. ZDH gratefully acknowledges a Graduate Research Fellowship award from the National Science Foundation (DGE-1650044) and the Georgia Tech-ORNL Fellowship. A portion of the electron microscopy work was performed at the Georgia Tech's Institute for Electronics and Nanotechnology, a member of the National Nanotechnology Coordinated Infrastructure, which is supported by the National Science Foundation (Grant ECCS-1542174).

Notes and references

1. C. M. Cobley, L. Au, J. Chen and Y. Xia, *Expert Opinion on Drug Delivery*, 2010, **7**, 577-587.
2. M. S. Yavuz, Y. Cheng, J. Chen, C. M. Cobley, Q. Zhang, M. Rycenga, J. Xie, C. Kim, A. G. Schwartz and L. V. Wang, *Nat. Mater.*, 2009, **8**, 935.
3. J. Yang, D. Shen, L. Zhou, W. Li, X. Li, C. Yao, R. Wang, A. M. El-Toni, F. Zhang and D. Zhao, *Chem. of Mat.*, 2013, **25**, 3030.
4. W. Li, X. Cai, C. Kim, G. Sun, Y. Zhang, R. Deng, M. Yang, J. Chen, S. Achilefu and L. V. Wang, *Nanoscale*, 2011, **3**, 1724.
5. H. Sun, J. Su, Q. Meng, Q. Yin, L. Chen, W. Gu, Z. Zhang, H. Yu, P. Zhang and S. Wang, *Adv. Funct. Mater.*, 2017, **27**, 9581.
6. H. Cheng, D. Huo, C. Zhu, S. Shen, W. Wang, H. Li, Z. Zhu and Y. Xia, *Biomater.*, 2018, *in press*.
7. J. Chen, C. Glaus, R. Laforest, Q. Zhang, M. Yang, M. Gidding, M. J. Welch and Y. Xia, *Small*, 2010, **6**, 811.
8. M. Hu, H. Petrova, J. Chen, J. M. McLellan, A. R. Siekkinen, M. Marquez, X. Li, Y. Xia and G. V. Hartland, *J. Phys. Chem. B*, 2006, **110**, 1520.
9. J. Chen, D. Wang, J. Xi, L. Au, A. Siekkinen, A. Warsen, Z.-Y. Li, H. Zhang, Y. Xia and X. Li, *Nano Lett.*, 2007, **7**, 1318.
10. Y. Wang, K. C. Black, H. Luehmann, W. Li, Y. Zhang, X. Cai, D. Wan, S.-Y. Liu, M. Li and P. Kim, *ACS Nano*, 2013, **7**, 2068.
11. J. Chen, F. Saeki, B. J. Wiley, H. Cang, M. J. Cobb, Z.-Y. Li, L. Au, H. Zhang, M. B. Kimmey and X. Li, *Nano Lett.*, 2005, **5**, 473.
12. E. C. Cho, C. Kim, F. Zhou, C. M. Cobley, K. H. Song, J. Chen, Z.-Y. Li, L. V. Wang and Y. Xia, *J. Phys. Chem. C*, 2009, **113**, 9023.
13. L. Sironi, S. Avvakumova, E. Galbiati, S. A. Locarno, C. Macchi, L. D'Alfonso, M. Ruscica, P. Magni, M. Collini and S. Romeo, *Proc. SPIE 9887*, 2016, 988721.
14. Y. Wang, Y. Liu, H. Luehmann, X. Xia, D. Wan, C. Cutler and Y. Xia, *Nano Lett.*, 2013, **13**, 581.
15. W. Li, P. K. Brown, L. V. Wang and Y. Xia, *Contrast Media Mol. Imaging*, 2011, **6**, 370.
16. X. Yang, M. Yang, B. Pang, M. Vara and Y. Xia, *Chem. Rev.*, 2015, **115**, 10410.

17. S. E. Skrabalak, J. Chen, Y. Sun, X. Lu, L. Au, C. M. Cobley and Y. Xia, *Acc. Chem. Res.*, 2008, **41**, 1587.
18. M. Hu, J. Chen, Z.-Y. Li, L. Au, G. V. Hartland, X. Li, M. Marquez and Y. Xia, *Chem. Soc. Rev.*, 2006, **35**, 1084.
19. J. Chen, B. Wiley, Z. Y. Li, D. Campbell, F. Saeki, H. Cang, L. Au, J. Lee, X. Li and Y. Xia, *Adv. Mater.*, 2005, **17**, 2255.
20. A. J. Powless, S. V. Jenkins, M. L. McKay, J. Chen and T. J. Muldoon, *Proc. SPIE*, 2015, **9339**, 93390B.
21. S. E. Skrabalak, L. Au, X. Lu, X. Li and Y. Xia, *Nanomed.*, 2007, **2**, 657.
22. S. Huang, S. Duan, J. Wang, S. Bao, X. Qiu, C. Li, Y. Liu, L. Yan, Z. Zhang and Y. Hu, *Adv. Funct. Mater.*, 2016, **26**, 2532.
23. K. H. Song, C. Kim, C. M. Cobley, Y. Xia and L. V. Wang, *Nano Lett.*, 2008, **9**, 183.
24. P. Shi, E. Ju, J. Ren and X. Qu, *Adv. Funct. Mater.*, 2014, **24**, 826.
25. X. Sun, J. Kim, K. D. Gilroy, J. Liu, T. A. König and D. Qin, *ACS Nano*, 2016, **10**, 8019.
26. X. Yang, K. D. Gilroy, M. Vara, M. Zhao, S. Zhou and Y. Xia, *Chem. Phys. Lett.*, 2017, **683**, 613.
27. S. Mallidi, T. Larson, J. Tam, P. P. Joshi, A. Karpiouk, K. Sokolov and S. Emelianov, *Nano Lett.*, 2009, **9**, 2825.
28. S. Mallidi, G. P. Luke and S. Emelianov, Trends in biotechnology, 2011, 29, 213-221.
29. W. Li and X. Chen, *Nanomed.*, 2015, **10**, 299.
30. A. S. Hannah, D. VanderLaan, Y.-S. Chen and S. Y. Emelianov, *Biomed. Opt. Express*, 2014, **5**, 3042.
31. J. Chen, M. Yang, Q. Zhang, E. C. Cho, C. M. Cobley, C. Kim, C. Glaus, L. V. Wang, M. J. Welch and Y. Xia, *Adv. Funct. Mater.*, 2010, **20**, 3684.
32. J. B. Herzog, M. W. Knight and D. Natelson, *Nano Lett.*, 2014, **14**, 499.
33. G. Baffou, R. Quidant and C. Girard, *App. Phys. Lett.*, 2009, **94**, 153109.
34. Y.-S. Chen, W. Frey, S. Kim, K. Homan, P. Kruizinga, K. Sokolov and S. Emelianov, *Opt. Express*, 2010, **18**, 8867.
35. S. Link and M. A. El-Sayed, International Reviews in Physical Chemistry, 2000, 19, 409.
36. H. Kurita, A. Takami and S. Koda, *Appl. Phys. Lett.*, 1998, **72**, 789.
37. P. V. Kamat, M. Flumiani and G. V. Hartland, *J. Phys. Chem. B*, 1998, **102**, 3123.

38. S. Link, C. Burda, M. Mohamed, B. Nikoobakht and M. A. El-Sayed, *J. Phys. Chem. A*, 1999, **103**, 1165.
39. B. G. Prevo, S. A. Esakoff, A. Mikhailovsky and J. A. Zasadzinski, *Small*, 2008, **4**, 1183.
40. S. Hashimoto, D. Werner and T. Uwada, *J. Photochem. and Photobio.*, C, 2012, **13**, 28.
41. ANSI Orlando: Laser Institute of America, American National Standard for Safe use of Lasers, ANSI Z136.1 American National Standards Institute, NewYork, 2000.
42. Q. Zhang, W. Li, L. P. Wen, J. Chen and Y. Xia, *Chem.-Eur. J.*, 2010, **16**, 10234.
43. S. E. Skrabalak, L. Au, X. Li and Y. Xia, *Nat. Proto.*, 2007, **2**, 2182.
44. O. Peña-Rodríguez, M. Caro, A. Rivera, J. Olivares, J. M. Perlado and A. Caro, *Optical Materials Express*, 2014, **4**, 403.
45. J.-M. Li, Y. Yang and D. Qin, *J. Mater. Chem. C*, 2014, **2**, 9934-9940.
46. Y.-S. Chen, W. Frey, S. Kim, P. Kruizinga, K. Homan and S. Emelianov, *Nano Lett.*, 2011, **11**, 348.
47. M. S. Sibbald, G. Chumanov and T. M. Cotton, *J. Phys. Chem.*, 1996, **100**, 4672.
48. F. Mafuné, J.-y. Kohno, Y. Takeda, T. Kondow and H. Sawabe, *J. Phys. Chem. B*, 2000, **104**, 9111.
49. T. Tsuji, K. Iryo, N. Watanabe and M. Tsuji, *Appl. Surf. Sci.*, 2002, **202**, 80.
50. A. Santagata, A. Guarnaccio, D. Pietrangeli, Á. Szegedi, J. Valyon, A. De Stefanis, A. De Bonis, R. Teghil, M. Sansone and D. Mollica, *J. Phys. D: Appl. Phys.*, 2015, **48**, 205304.
51. M. Delmée, G. Mertz, J. Bardon, A. Marguier, L. Ploux, V. Roucoules and D. Ruch, *J. Phys. Chem. B*, 2017, **121**, 6646.
52. V. Amendola and M. Meneghetti, *Phys. Chem. Chem. Phys.*, 2009, **11**, 3805.
53. V. Amendola and M. Meneghetti, *Phys. Chem. Chem. Phys.*, 2013, **15**, 3027.
54. L. J. Lewis, P. Jensen and J.-L. Barrat, *Phys. Rev. B*, 1997, **56**, 2248.
55. F. Ercolessi, W. Andreoni and E. Tosatti, *Phys. Rev. Lett.*, 1991, **66**, 911.
56. S. Link, Z. L. Wang and M. A. El-Sayed, *J. Phys. Chem. B*, 2000, **104**, 7867.
57. G. González-Rubio, P. Díaz-Núñez, A. Rivera, A. Prada, G. Tardajos, J. González-Izquierdo, L. Bañares, P. Llombart, L.G. Macdowell, M.A. Palafox, L.M. Liz-Marzán, O. Peña-Rodríguez, and A. Guerrero-Martínez, *Science*, 2017, **358**, 640.
58. T. S. Ahmadi, S. L. Logunov and M. A. El-Sayed, *J. Phys. Chem.*, 1996, **100**, 8053.
59. J. H. Hodak, I. Martini and G. V. Hartland, *J. Phys. Chem. B*, 1998, **102**, 6958.

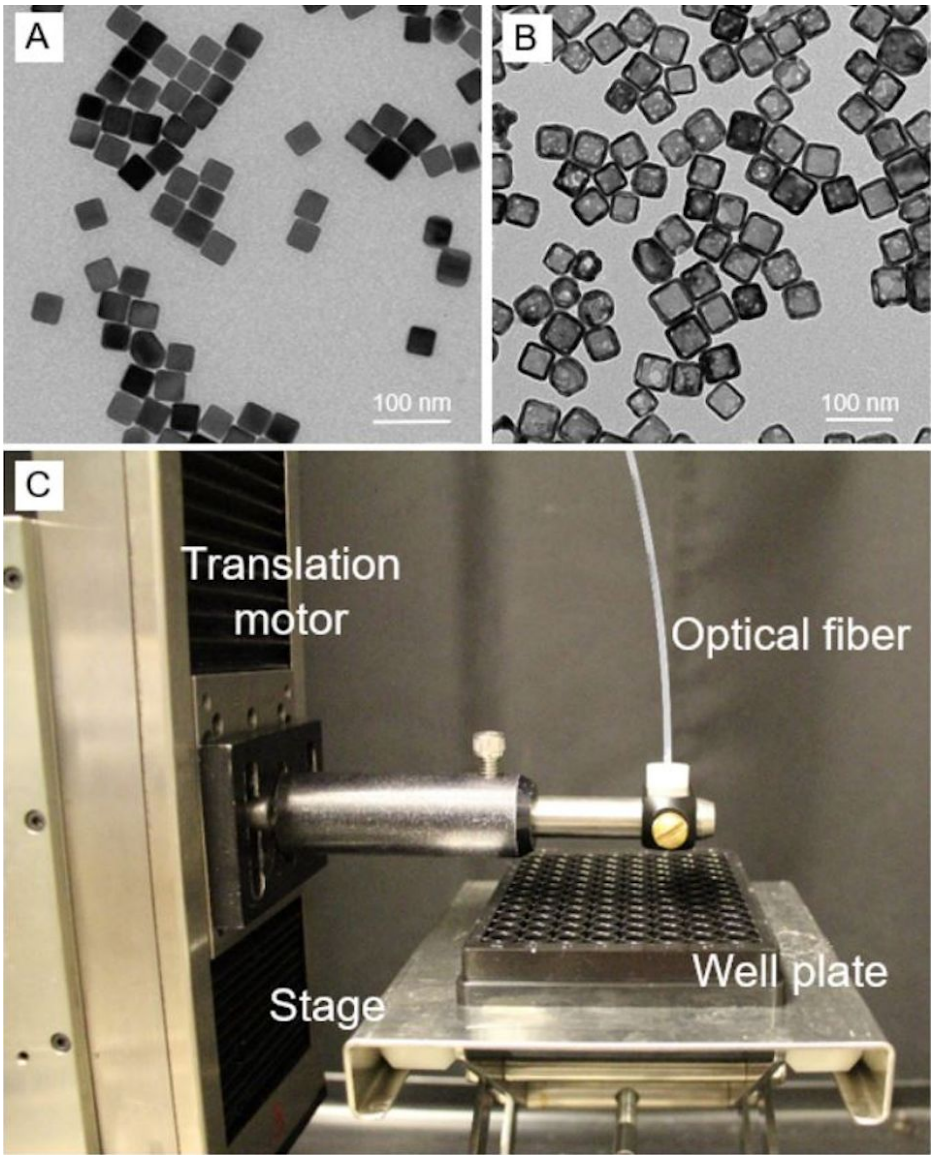

Figure 1. TEM images of the (A) Ag nanocubes and (B) Au-Ag nanocages. (C) Photograph of the setup for pulsed laser irradiation experiments.

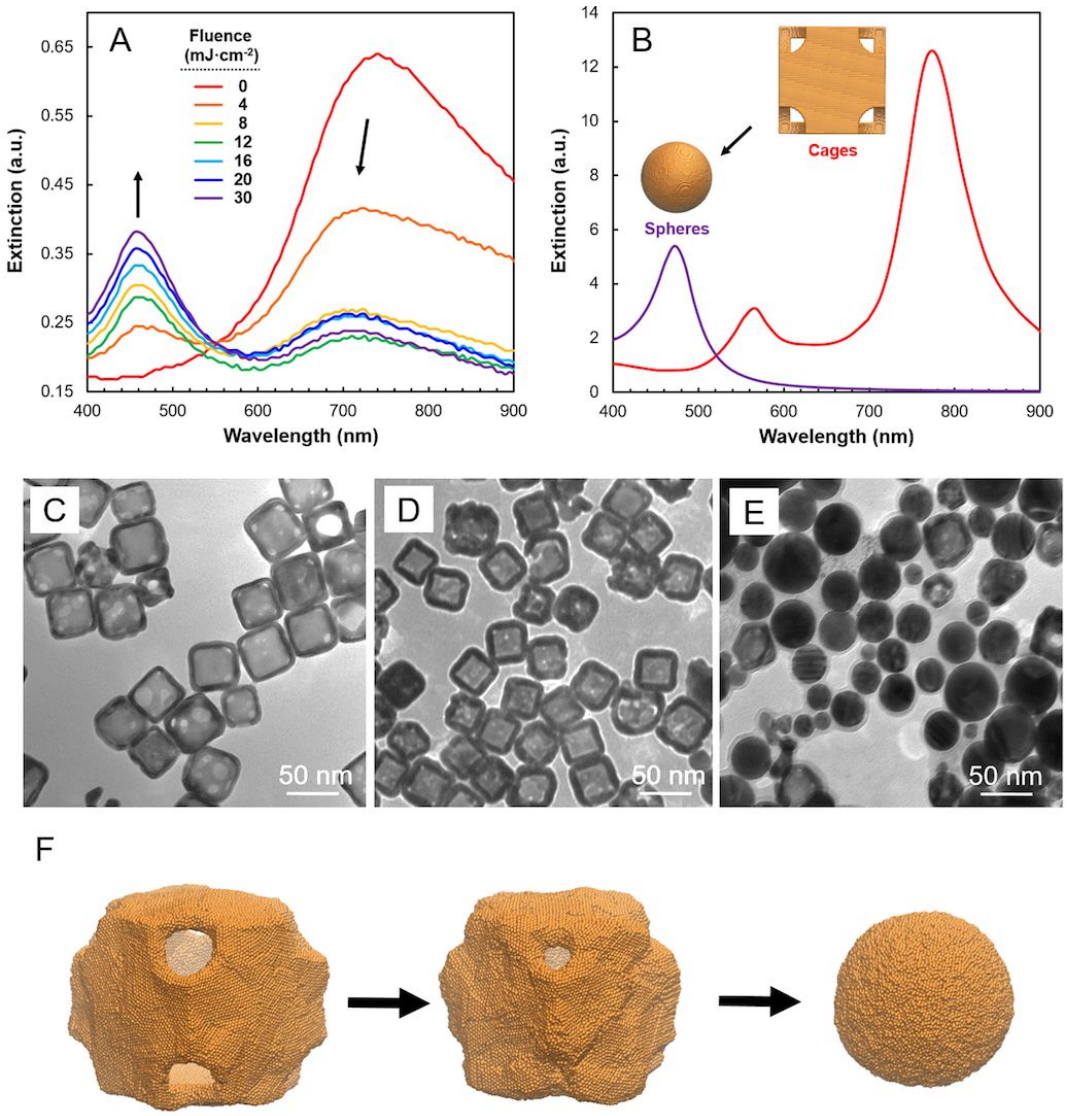

Figure 2. Optical and morphological changes to the nanocages as a function of laser irradiation fluence. (A) UV-vis absorbance spectra recorded from aqueous suspensions of the as-prepared Au-Ag nanocages and after 300 pulses at different laser fluences. (B) Simulated UV-vis spectra for the Au-Ag nanocage (with an edge length of 47 nm and a wall thickness of 4 nm) and pseudo-spherical solid nanoparticle with a diameter of 41 nm. (C-E) TEM images of (C) the as-prepared nanocages and the products after 300 laser pulses at (D) 4 and (E) 20 mJ cm^{-2}, respectively. (F) Schematic illustration showing the morphological evolution from a hollow nanocage to pseudo-spherical, solid nanoparticle after exposure to pulsed laser irradiation.

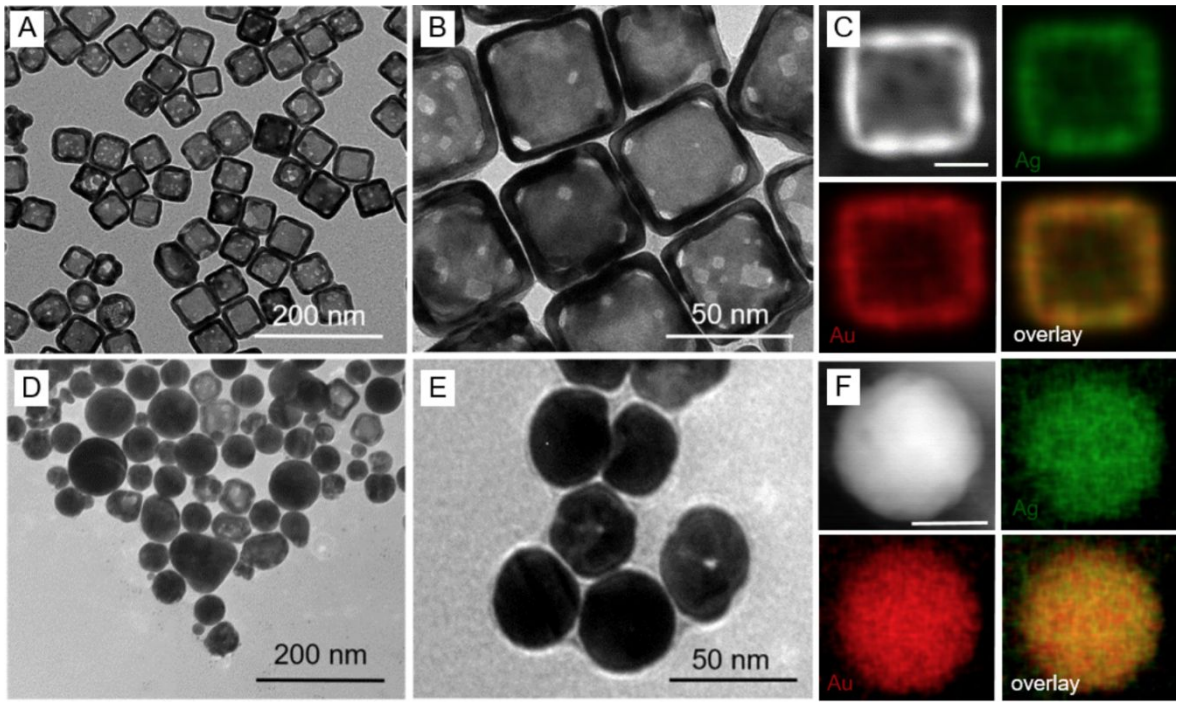

Figure 3. (A, B) TEM images of representative Au-Ag nanocages and (C) EDS elemental mapping for Ag and Au in an individual nanocage (scale bar: 25 nm). (D, E) TEM images of representative pseudo-spherical, solid nanoparticles after 300 pulses at a laser fluence of 12 mJ cm^{-2} and (F) EDS elemental mapping for Ag and Au in a representative solid nanoparticle (scale bar: 25 nm).

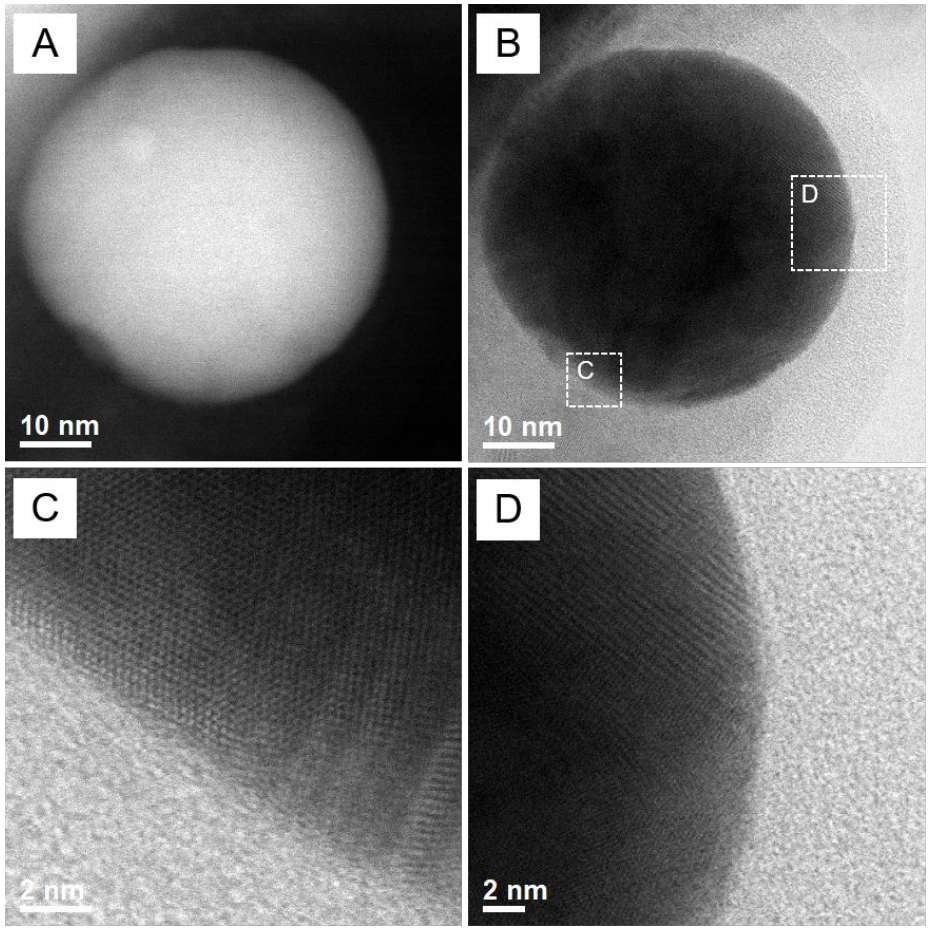

Figure 4. (A) HAADF-STEM and (B) bright-field STEM images of a pseudo-spherical, solid nanoparticle obtained from the nanocage after 300 pulses at a laser fluence of 12 mJ cm^{-2}. (C, D) Bright-field STEM images of the areas marked in (B).

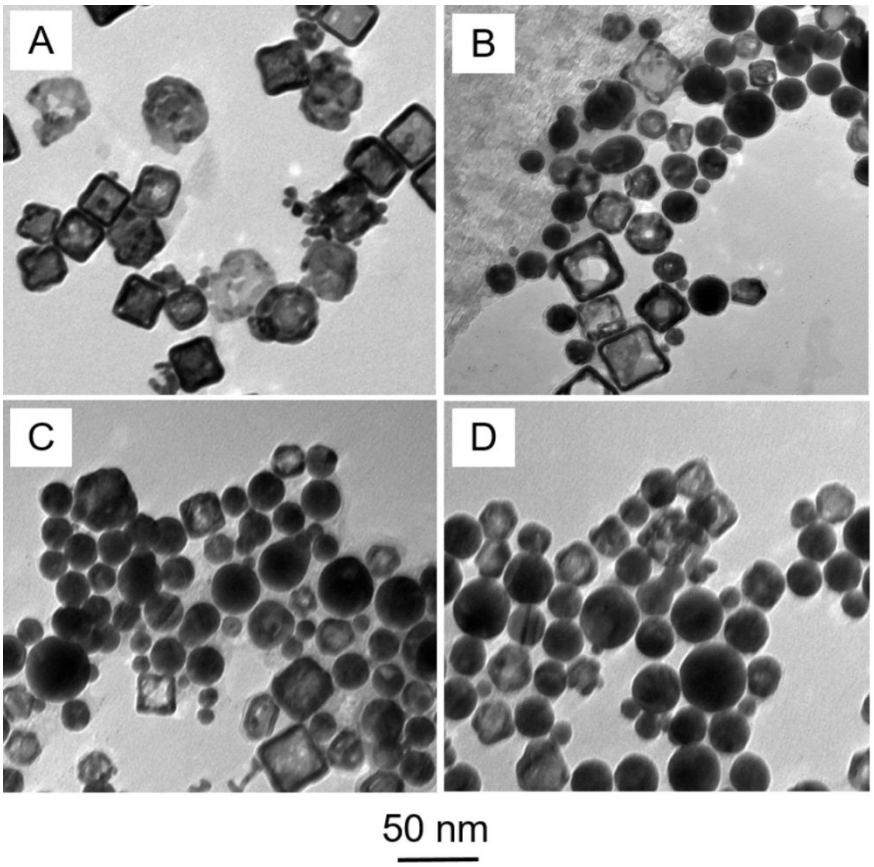

Figure 5. TEM images of the nanoparticles obtained from the nanocages after laser exposure at 8 mJ cm^{-2} for (A) 5, (B) 50, (C) 150, and (D) 300 pulses, respectively.

TOC entry

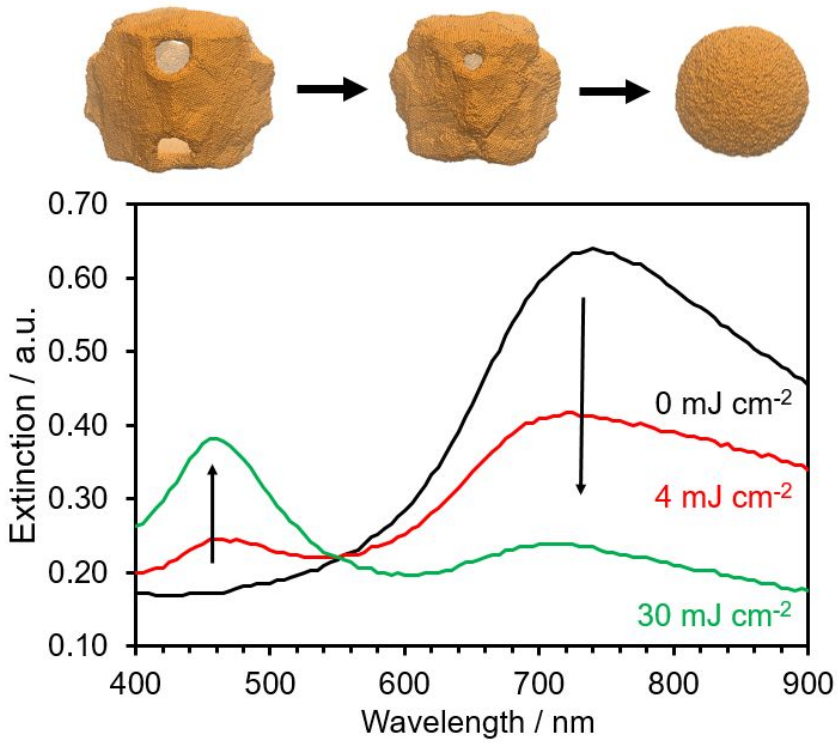

Pulsed laser irradiation can photothermally transform Au-Ag nanocages into pseudo-spherical, solid nanoparticles. The results may have implications for the future use of Au-Ag nanocages in biomedicine, catalysis, and sensing.